Available online at www.sciencedirect.com
SCIENCE DIRECT
Journal of Colloid and Interface Science 297 (2006) 235–243
JOURNAL OF Colloid and Interface Science
www.elsevier.com/locate/jcis

A novel organoclay with antibacterial activity prepared from montmorillonite and Chlorhexidini Acetas

Hongping He [a,b], Dan Yang [a,c], Peng Yuan [a], Wei Shen [a], Ray L. Frost [b,*]

[a] *Guangzhou Institute of Geochemistry, Chinese Academy of Sciences, Guangzhou 510640, China*
[b] *Inorganic Materials Research Program, School of Physical and Chemical Sciences, Queensland University of Technology, PO Box 2434 GPO, Brisbane, QLD 4001, Australia*
[c] *Graduate School of Chinese Academy of Sciences, Beijing 100039, China*

Received 31 August 2005; accepted 4 October 2005
Available online 23 November 2005

Abstract

A series of novel organoclays with antibacterial activity were synthesized using Ca-montmorillonite and Chlorhexidini Acetas (CA) by ion-exchange. The resultant organoclays were characterized using X-ray diffraction (XRD), high-resolution thermogravimetric analysis (HRTG) and Fourier transform infrared spectroscopy (FTIR). Their antibacterial activity was assayed by so-called halo method. In the organoclays prepared at low CA concentration, CA ions within the clay interlayer adopt a lateral monolayer while a 'kink' state or a special state with partial overlapping of the intercalated CA in the organoclays prepared at 1.0–4.0 CEC. HRTG analysis demonstrates that CA located outside the clay interlayer exists in all synthesized organoclays, resulting from the complex molecular configuration of CA. The dramatic decrease of the surface adsorbed water and interlayer water is caused by the surface property transformation and the replacement of hydrated cations by cationic surfactant. These observations are supported by the results of FTIR. Antibacterial activity test against *E. coli* demonstrates that the antibacterial activity of the resultant organoclays strongly depends on the content of CA. Meanwhile, the resultant organoclay shows a long-term antibacterial activity that can last for at least one year. These novel organoclays are of potential use in synthesis of organoclay-based materials with antibacterial activity.

Keywords: Organoclay; Chlorhexidini Acetas; Antibacterial materials; Antibacterial activity; Halo method; Nanocomposite

1. Introduction

In recent years organoclays have attracted great interest because of their academic and industrial importance [1,2]. Organoclay-based nanocomposites exhibit remarkable improvements in properties when compared with virgin polymer or conventional micro- and macrocomposites. These improvements include increased strength and heat resistance, decreased gas permeability and flammability, and increased biodegradability of biodegradable polymer [2]. Another important application for organoclays is in adsorption such as in pollution prevention and environmental remediation such as treatment of chemical spills, wastewater treatment and hazardous waste landfills and others [3,4]. The aforementioned applications strongly depend on the structure and properties of the organoclays. Hence, various techniques have been used to explore the nanochemistry and microstructure of organoclays, including X-ray diffraction (XRD) [5,6], Fourier transform infrared spectroscopy (FTIR) [7–9], Raman [10], thermal analysis [11–16], ^{13}C magic-angle-spinning nuclear-magnetic resonance (^{13}C MAS NMR) [17,18], and electron microscopy [19–21]. On the basis of the measured basal spacings and the length of the alkyl chains, various arrangement models have been proposed for the intercalated surfactants, including lateral-monolayer, lateral-bilayer, pseudo-trilayer, paraffin-monolayer and paraffin-bilayer [5,6].

Meanwhile, the synthesis and application of clay-based antibacterial materials have attracted great interest due to the worldwide concern about public health [22]. According to the type of antibacterial ions used, antibacterial materials could be divided into two basic types, i.e., inorganic and organic antibac-

* Corresponding author.
E-mail address: r.frost@qut.edu.au (R.L. Frost).

0021-9797/$ – see front matter
doi:10.1016/j.jcis.2005.10.031

terial materials. In the synthesis of clay-based inorganic antibacterial materials, most antibacterial inorganic cations used are heavy metals such as Ag^+, Cu^{2+} and Zn^{2+} [23–27]. Each of these cations can function as an antibacterial agent. However, a lot of problems and/or disadvantages arise in the synthesis and application of inorganic antibacterial materials with heavy metals, including: (1) An accumulation of heavy metals will result in serious environmental problems and may be harmful to humans in the case of high metal concentration; (2) Ag^+ is not stable in aqueous solution. It tends to be reduced to Ag^0 when exposed to light or heat or to react with anions (e.g., Cl^-, HS^-, SO_4^{2-}) in natural water, forming insoluble compounds and losing their antibacterial activity [26]; (3) heavy metals are easy to be fixed into the hexagonal cavities and the octahedral vacancies in montmorillonite [28], resulting in a decrease of the antibacterial activity.

Hence, despite the relative low stability compared with inorganic antibacterial materials (e.g., low decomposition temperature, low melting point) [25], organic antibacterial materials show some advantages in their synthesis and application. For example, the synthesis and storage conditions of organic antibacterial materials are not as strict as those for inorganic antibacterial materials. What is even more important, organic antibacterial materials display organophilicity, i.e., the compatibility with organic matrix such as textile, paints, polymer, etc. Here, a very interesting and novel concept is proposed in which a new family of organoclay-based materials (e.g., nanocomposites, paintings) with antibacterial property could be synthesized using clays modified by special surfactants that have antibacterial activity.

In this study, a kind of novel organoclay with antibacterial activity was synthesized using Ca-montmorillonite and Chlorhexidini Acetas ($C_{22}H_{30}N_{10}Cl_2{\cdot}2C_2H_4O_2$). Chlorhexidini Acetas (abbreviated as CA hereafter) is a kind of bivalent cationic surfactant with efficiency as an antibacterial ion. In fact, CA has been widely used for diminishing inflammation, disinfecting and washing the surface of a wound [29]. In this paper, the structure of the resultant organoclays was characterized by X-ray diffraction (XRD), high-resolution thermogravimetric analysis (HRTG) and Fourier transform infrared spectroscopy (FTIR). Their antibacterial activity was assayed by so-called halo method. This is a strategic step for the preparation of novel organoclay-based materials with antibacterial activity.

2. Experimental

2.1. Materials

Ca-montmorillonite (CaMt) from Hebei, China, was purified by a conventional sedimentation method. The <5-μm size fraction was collected and dried at 90 °C. Then, the sample was ground through a 200 mesh sieve and sealed in a glass bottle for further use. The cation exchange capacity (CEC) of CaMt is 80.1 meq/100 g, determined by NH_4^+ exchanging method [28]. The chemical formula of CaMt is $(Na_{0.05}Ca_{0.18}Mg_{0.10})[Al_{1.58}Fe_{0.03}Mg_{0.39}][(Si_{3.77}Al_{0.23})]O_{10}(OH)_2{\cdot}nH_2O$, calculated from the chemical analysis result.

Chlorhexidini Acetas ($C_{22}H_{30}N_{10}Cl_2{\cdot}2C_2H_4O_2$) was provided by Jiutai Pharmaceutical Co. Ltd., Jinzhou, China, with a purity of 98%.

2.2. Synthesis of organoclays

The syntheses of montmorillonite/Chlorhexidini-Acetas organoclays were performed by the following procedure. 2 g of CaMt was dispersed in about 30 ml of distilled water and a desired amount of CA was dissolved in 70 ml of ethanol. The concentrations of CA varied from 0.2 to 4.0 CEC of montmorillonite. Then, the two solutions were mixed together and stirred for 2 days at room temperature. All products were washed twelve times with ethanol, dried at 105 °C and ground in an agate mortar to pass through a 200 mesh sieve. The organoclay prepared at the CA concentration of 0.2 CEC was marked as CaMt-0.2CEC and the others were marked in a similar way.

2.3. Characterization

Powder X-ray diffraction (XRD) patterns were recorded between 1.5° and 20° (2θ) at a scanning speed of 2°/min using Rigaku D/max-1200 diffractometer with Cu K_α radiation.

High-resolution thermogravimetric (HRTG) analysis was performed on a TA Instruments, Inc., Q500 thermobalance. Samples were heated from room temperature to 1000 °C at a heating rate of 10 °C/min with a resolution of 6 °C under nitrogen atmosphere (80 cm^3/min). Approximately 30 mg of finely ground sample was heated in an open platinum crucible.

The Fourier transform infrared spectroscopy (FTIR) spectra using ATR technique were recorded on Nicolet Nexus 870 Fourier transform infrared spectrometer with a Diamond Attenuated Total Reflectance (ATR) Smart Accessory. 64 scans were collected for each measurement over the spectral range of 525–4000 cm^{-1} with a resolution of 4 cm^{-1}.

2.4. Antibacterial activity test

Antibacterial activity of the resultant organoclays was assayed by so-called halo method as follows [30]. A melted beef agar medium was poured in a Petri dish and solidified. Then, the medium containing bacteria (1×10^6 cells of *E. coli* per ml) was layered over it. The organoclay was put on the surface and then incubated. Incubation conditions were 1 day at 37 °C. Antibacterial activity was evaluated by the transparent halo circle around the organoclay specimen after incubation. That is to say, when an agent has antibacterial activity, the halo circle is formed along the periphery of the organoclay. When materials have an excellent antibacterial activity, the halo ring is very wide. All glassware used in this study was sterilized in the autoclave at 120 °C for 30 min before each experiment to exclude any possible microbial disturbance.

3. Results and discussion

3.1. X-ray diffraction (XRD)

One well-established method for characterizing clays and organoclays is the use of X-ray diffraction. This technique enables to determine the expansion of the clay as well as the crystallite size. Fig. 1 shows XRD patterns of CaMt and the resultant organoclays. The basal spacing (d_{001}) of CaMt is 1.53 nm, a characteristic d value for Ca-montmorillonite. The d_{001} value of CaMt-0.2CEC is 1.50 nm, similar to that of CaMt. On the basis of its basal spacing, it is difficult to determine whether CA has been intercalated into the montmorillonite interlayer. However, both TG and FTIR analyses demonstrate that CA has been intercalated into montmorillonite interlayer (see below). For the organoclays prepared at the CA concentrations of 1.0–4.0 CEC, their basal spacings are similar and locate at 1.65–1.67 nm. This

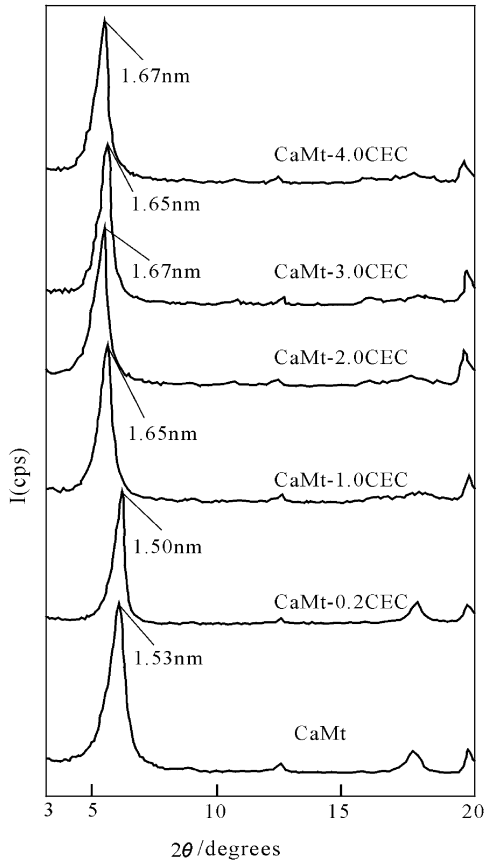

Fig. 1. X-ray diffraction patterns of CaMt and the resultant organoclays.

d value is obviously lager than that of CaMt, indicating that CA has entered into the clay interlayer.

As is well known, the layer thickness of montmorillonite is ca. 0.97 nm, hence the interlayer height of CaMt-0.2CEC should be ca. 0.53 nm. This value almost equals to the height of a phenol ring in CA (0.5 nm) as shown in Fig. 2 (both the heights of $–CH_2–$ and –NH– groups are less than 0.5 nm). Hence, a lateral monolayer arrangement is supposed for the intercalated CA in the montmorillonite interlayer. For CaMt-1.0CEC, CaMt-2.0CEC, CaMt-3.0CEC, and CaMt-4.0CEC, the interlayer height is about 0.7 nm. Obviously, this interlayer distance is bigger than that when CA adopts a lateral monolayer arrangement (0.5 nm), but smaller than that of a lateral bilayer arrangement (ca. 1 nm). Favre and Lagaly [31] proposed that this d value corresponds to a 'kink' structure. Recently, our molecular modeling of organoclays demonstrates a transition structure from lateral-monolayer to lateral-bilayer, in which a partial overlapping of organic molecules was observed [32]. In the present study, even when the CA concentration increased to 4.0 CEC, the basal spacing of the resultant antibacterial compound still remained at ca. 1.67 nm. This is very different from those of quaternary alkylammonium modified montmorillonites [5,6], in which various surfactant arrangement models (e.g., lateral monolayer, lateral bilayer, pseudotrilater, paraffin monolayer, paraffin bilayer) were observed, depending on the surfactant concentration in the preparation solution and the content of the intercalated surfactant. The similar basal spacings for the resultant organoclays prepared at 1.0–4.0 CEC should be attributed to the complex structure of CA molecules with a phenol ring at the two opposite ends, respectively, resulting in the difficulty for intercalation.

3.2. Thermal analysis

One method for the characterization of the organoclay is the use of thermal analysis techniques. Such techniques determine the thermal stability of the organoclay and the thermal decomposition mechanisms. The DTG curve of CaMt (shown in Fig. 3) displays four peaks at 30–42, 115, 633 and 915 °C, respectively. The peaks at 30–42, 115, and 633 °C correspond to the loss of surface adsorbed water, hydrated water of the interlayer cations and the structural hydroxyls, respectively [16]. The peak at ca. 915 °C should be attributed to phase transformation from montmorillonite to spinel, cristobalite, mullite, and/or pyroxenes (enstatite) [33].

However, the DTG curves of the CA modified montmorillonites display several peaks around 218, 294, 375, 450 and

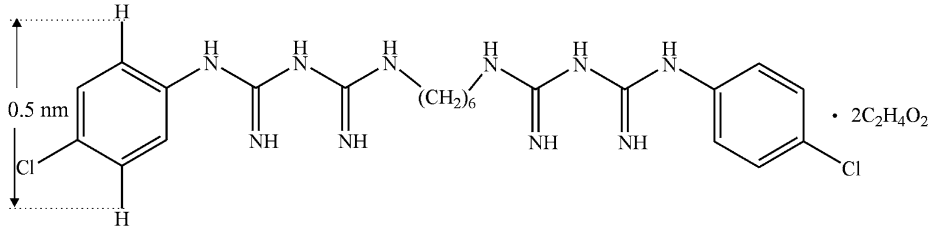

Fig. 2. The molecular configuration of Chlorhexidini Acetas.

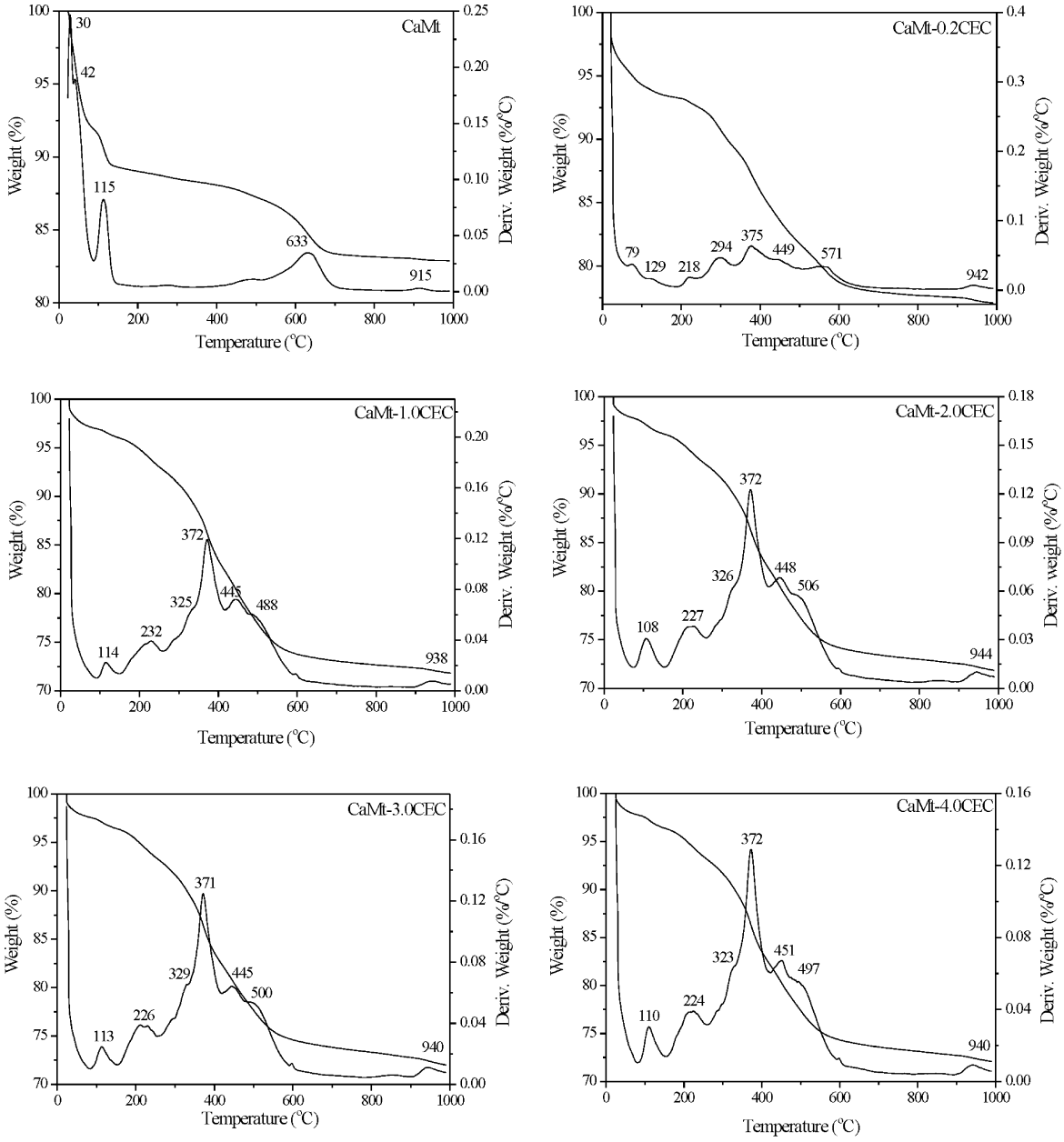

Fig. 3. TG and DTG curves of CaMt and the resultant organoclays.

500 °C. As indicated by the TG and DTG curves of CaMt, montmorillonite is thermally stable in the temperature range of 200–500 °C. Hence, the weight loss in this temperature range should be attributed to the evaporation and/or decomposition of CA within the organoclays. For CaMt-0.2CEC, the DTG curve displays three prominent peaks at 218, 294 and 375 °C and a shoulder at 450–570 °C. This is similar to the DTG curves of quaternary alkylammonium modified montmorillonites prepared at relatively higher concentrations of surfactant [16]. The peak at 218 °C corresponds to the evaporation of physically adsorbed CA while the peaks at 294 and 375 °C to the decomposition of the intercalated CA within the clay interlayer [12–16]. The mass loss at 450–570 °C is related to the oxidation of residual organic with the organoclays [13]. The thermal analysis demonstrates that CA has been intercalated into montmorillonite interlayer in CaMt-0.2CEC. However, as demonstrated by the TG and DTG curves, a minor content of CA (ca. 1 wt%, corresponding to the weight loss around 218 °C) is locating outside the clay layer. This is very different from the quaternary alkylammonium modified montmorillonite prepared at the same surfactant concentration [16], i.e., all surfactants are intercalated into clay interlayer in the latter case. This should be attributed to the molecular configuration of surfactant as in the above discussion.

The TG curves of CaMt-1.0CEC, CaMt-2.0CEC, CaMt-3.0CEC and CaMt-4.0CEC show a larger mass loss corresponding to the evaporation and/or decomposition of CA, reflecting that there is more CA in the resultant organoclays. The CA contents in the resultant organoclays are summarized in Table 1, deduced from the corresponding HRTG curves and corrected

Table 1
The CA loadings (wt%) in the resultant organoclays synthesized at different CA concentrations

CaMt-0.2CEC	CaMt-1.0CEC	CaMt-2.0CEC	CaMt-3.0CEC	CaMt-4.0CEC
10.73	19.01	18.86	18.82	18.95

Note. The CA loadings are deduced from the corresponding HRTG curves, corrected with regard to the appropriate mass fraction of montmorillonite in the compounds for the mass loss associated with dehydroxylation of montmorillonite.

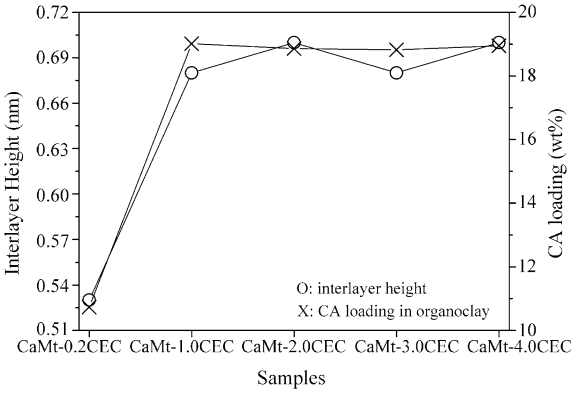

Fig. 4. The relationship between the interlayer height and the CA loading in the organoclays.

with regard to the appropriate mass fraction of montmorillonite in the organoclays for the mass loss associated with dehydroxylation of montmorillonite. Here, it can be found that the CA contents in CaMt-1.0CEC, CaMt-2.0CEC, CaMt-3.0CEC and CaMt-4.0CEC are similar (ca. 19 wt%). Fig. 4 represents the relationship between the interlayer height and the CA loading in the resultant organoclays. Obviously, the interlayer height of the organoclays strongly depends on the CA loading.

As shown by the TG and DTG curves of CaMt and the resultant organoclays, the amounts of surface adsorbed water and the hydrated water strongly depend on the CA content in the organoclays. The TG curve of CaMt displays two prominent mass loss stages at ca. 40 and 115 °C, related to the loss of surface adsorbed water (ca. 8.3 wt%) and hydrated water (ca. 2.8 wt%) in the clay interlayer [16]. With the intercalation of CA, both the amounts of surface adsorbed water and the hydrated water decrease dramatically. The DTG curve of CaMt-0.2CEC shows a weak peak corresponding to a mass loss of surface adsorbed water (about 4.4 wt%) while those of CaMt-1.0CEC, CaMt-2.0CEC, CaMt-3.0CEC and CaMt-4.0CEC do not show any related peaks. Meanwhile, the loss of the hydrated water in the organoclays also decreases to 1–2 wt%. The former should be attributed to the surface property transformation from hydrophilic (montmorillonite) to hydrophobic (organoclay) while the latter results from the replacement of the interlayer hydrated cations by cationic surfactant. This observation is in accord with the FTIR results (see below). The surface property transformation of clays, from hydrophilic to hydrophobic, is a strategic step for the preparation of polymer/layer silicate nanocomposites.

3.3. Fourier transform infrared spectroscopy (FTIR)

FTIR spectroscopy measures the molecular vibrations of the organoclay. The changes in the structure of the organoclay will be observed through changes in the infrared spectra. In comparison to thermal analysis where bulk properties are measured, infrared spectroscopy determines changes in the molecular structure. Figs. 5 and 6 represent the H–O–H bending region (1600–1700 cm^{-1}) and O–H stretching region of H_2O (3100–3700 cm^{-1}) in the FTIR spectra of CaMt and the resultant organoclays. As shown in Fig. 5, the position of the band, related to the ν_2(H–O–H) bending vibration of water molecules adsorbed on montmorillonite, shifted from 1630 cm^{-1} (for CaMt) to ca. 1636 cm^{-1} (for the resultant organoclays). Simultaneously, the intensity of this band decreases significantly. The decrease of the band intensity reflects that the amount of hydrogen bonded H_2O molecules presenting in the organoclays is reduced with the intercalation of surfactant. This results from the transformation of the surface property from hydrophilic to hydrophobic and replacement of the hydrated interlayer cations with the intercalation of surfactant. H_2O is not easily to be sorbed by surfactant modified montmorillonite except those coordinated H_2O molecules of the retained cations in the interlayer. Those coordinated H_2O molecules are restricted in their ability to form hydrogen bonds with adjacent H_2O molecules [34].

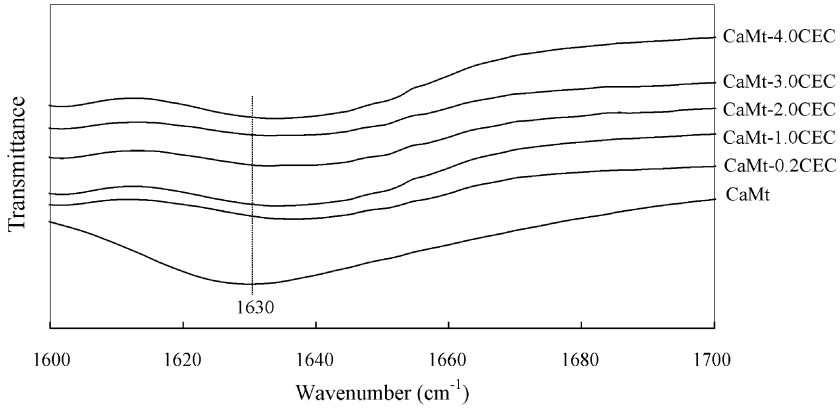

Fig. 5. FTIR spectra of the H–O–H bending region of H_2O (1600–1700 cm^{-1}).

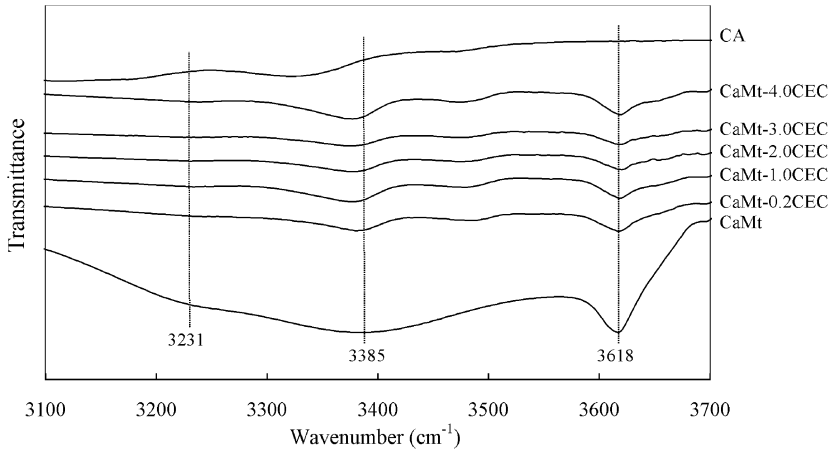

Fig. 6. FTIR spectra of the O–H stretching region of H_2O (3100–3700 cm^{-1}).

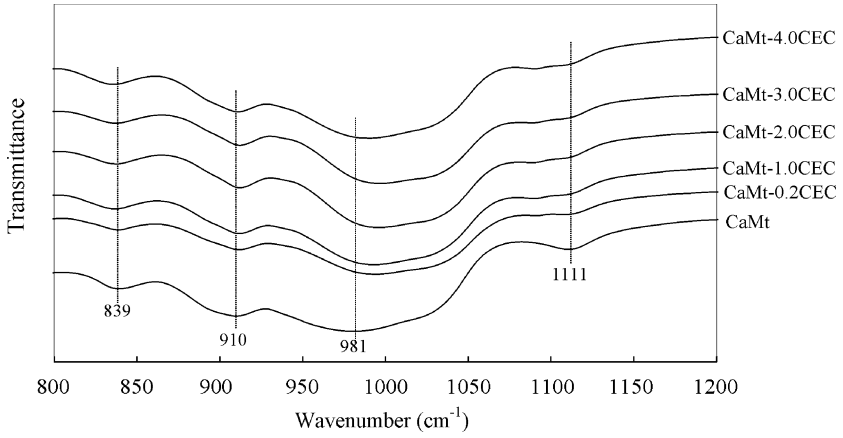

Fig. 7. FTIR spectra corresponding to the structural units in tetrahedral- and octahedral-sheets of montmorillonite (800–1200 cm^{-1}).

In the range of 3100–3700 cm^{-1}, the FTIR spectrum of CaMt (Fig. 6) displays a strong band at 3618 cm^{-1} due to the OH stretching vibrations of the structural OH groups and a broad band at 3385 cm^{-1} with a shoulder at ca. 3231 cm^{-1} due to sorbed water. The latter two bands are attributed to the overlapping antisymmetric ν_3 and symmetric ν_1(H–O–H) stretching vibrations of H-bonded water [35] and an overtone ($2\nu_2$) of the bending mode of cation hydration water [36], respectively. The position of the sharp band corresponding to the OH stretching vibrations of the structural OH groups shows independence of the surfactant intercalation whereas that of the broad band at ca. 3385 cm^{-1} is due to sorbed water which shifts to lower frequency after the intercalation of CA.

The above-mentioned FTIR bands demonstrate that the intercalation of CA has a prominent effect on the sorbed water and hydrated water in the interlayer, but little on the structural OH groups. This is in harmony with the TG analysis and similar to our previous study about $HDTMA^+$ modified montmorillonites [9,10].

With the decrease of H_2O content in montmorillonite, the frequency shift trends of the H–O–H bending and stretching vibrations of organoclays in the present study are contrary to those of various metals exchanged montmorillonites in most studies reported in the literature [35,37–39]. These previous studies reported that the position of the ν_2 mode of H_2O decreases and H_2O-stretching band shifts to higher wavenumber upon lowering the H_2O content in metal-exchanged montmorillonite. Yan and co-workers [37,38] interpreted the decrease in frequency of the ν_2 mode to a coupling between H_2O molecules and the Si–O stretching vibrations of the 2:1 layer through the formation of hydrogen bonds. The shift of the ν_2 mode to lower frequency, however, is not consistent with the observed frequency shift of the ν(OH) modes of sorbed H_2O reported here. Our results are similar to those reported by Xu and coworkers [34] and indicate that H_2O is less hydrogen bonded in the case of low-H_2O content. H_2O molecules clustered around exchangeable cations are polarized by the close proximity to the exchangeable cation with the oxygen of the H_2O directed toward the metal cation [34]. Furthermore, the intercalation of CA ions will increase such polarization. Thus, a decrease in hydrogen bonding is consistent with isolated hydrated clusters of the residual metal cations within the montmorillonite interlayer.

Fig. 7 displays the FTIR spectra of CaMt and the resultant organoclays in the range of 800–1000 cm^{-1}. The bands at 1111 and 981 cm^{-1} in the spectrum of CaMt correspond to Si–O and Si–O–Si stretching vibrations of montmorillonite [36]. After the intercalation of CA, the band at 981 cm^{-1} shifts to higher frequency (993–990 cm^{-1}) while the band at 1111 cm^{-1} be-

comes a shoulder. However, the bands at 910 and 839 cm^{-1}, corresponding to Al–OH and Mg–O bending vibrations, show independence of the surfactant intercalation. These results demonstrate that the intercalation of surfactant has a prominent effect on the atomic environment in the Si–O tetrahedral sheet but little on that of Al(Mg)–O octahedral sheet. This results from the various distances between CA and the different structural sheets (Si–O tetrahedral sheet and Al(Mg)–O octahedral sheet). As we know, montmorillonite has a TOT structure with two Si–O tetrahedral sheets sandwiching a Al(Mg)–O octahedral sheet. Accordingly, in the clays intercalated with cationic surfactant, the head of the surfactant cation with positive charge contacts directly with the clay surface (Si–O tetrahedral sheet) by the strong electrostatic force as indicated by molecular modeling [32,40,41]. However, the Al(Mg)–O octahedral sheet is separated from the intercalated surfactant by the Si–O tetrahedral sheet, i.e., the interaction between the intercalated surfactant and the Al(Mg)–O sheet is very weak. This results in the variations of the interaction force between CA and different montmorillonite structural sheets, consequently leading to different influences on the structural units in the resultant organoclays. The different changes of band frequency for the units in tetrahedral- and octahedral-sheets strongly suggest that CA has entered into montmorillonite interlayer.

Previous studies [8,9,42,43] have shown that the wavenumbers of the CH_2 stretching vibration bands are extremely sensitive to its local environmental changes. The FTIR spectrum of CA displays two bands at 2933 and 2858 cm^{-1}, corresponding to the antisymmetric and symmetric CH_2 stretching modes of CA, respectively (as shown in Fig. 8). After intercalation, the band corresponding to the antisymmetric CH_2 stretching mode, shifts to 2943 cm^{-1} for CaMt-0.2CEC, reflecting that the conformation of the intercalated CA becomes disordered when compared with that of a neat CA [8,9,42]. However, in the FTIR spectra of the organoclays prepared at 1.0–4.0 CEC, the frequency of this band is similar and shifts to a lower wavenumber (ca. 2938 cm^{-1}), reflecting an increase of the conformation order for the intercalated surfactant (compared with that of CaMt-0.2CEC). As demonstrated by TG analysis, the amounts of the intercalated surfactant in CaMt-1.0CEC, CaMt-2.0CEC, CaMt-3.0CEC and CaMt-4.0CEC are similar (ca. 19 wt% as shown in Table 1) but higher than that in CaMt-0.2CEC (10.7 wt%). Here, it could be found that the order of the intercalated CA strongly depends on the surfactant packing density within the montmorillonite interlayer, similar to the previous reports about quaternary ammonium [8,9]. However, contrary to the antisymmetric CH_2 stretching mode, the frequency of the symmetric CH_2 stretching mode remains at ca. 2859 cm^{-1} for all resultant organoclays, similar to that of CA (2858 cm^{-1}). This reflects that the antisymmetric CH_2 stretching mode is more sensitive to its local environment than the symmetric CH_2 stretching mode is, as elucidated by our previous FTIR and Raman studies of $HDTMA^+$ modified montmorillonites [9,10].

The FTIR spectra provide not only the detailed microstructural information about CA intercalated montmorillonites but also the confident evidence that CA has been intercalated into the montmorillonite interlayer as demonstrated by XRD and TG analyses.

3.4. Antibacterial test

The halo test results of CaMt and the resultant organoclays are shown in Fig. 9. Both the raw montmorillonites (CaMt) and

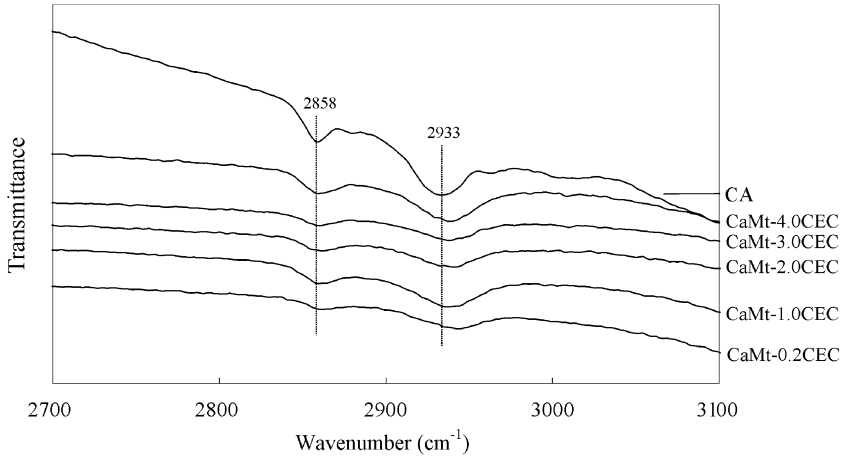

Fig. 8. FTIR spectra of organoclays in the range of 2800–3000 cm^{-1}.

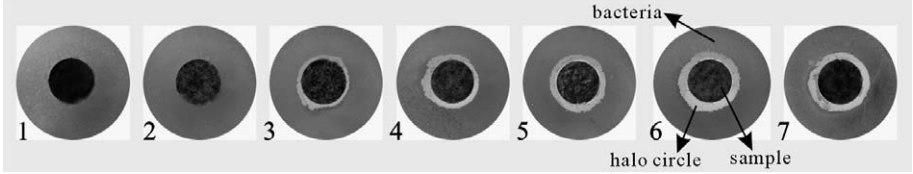

Fig. 9. Halo test results of CaMt and the resultant organoclays. (1) CaMt; (2) CaMt-0.2CEC; (3) CaMt-1.0CEC; (4) CaMt-2.0CEC; (5) CaMt-3.0CEC; (6) CaMt-4.0CEC; (7) CaMt-2.0CEC (test conducted after one year).

CaMt-0.2CEC show no halo circle for *E. coli*, reflecting no antibacterial activity for these materials. However, the organoclays synthesized at the CA concentration of 1.0–4.0 CEC, display a very clear halo circle around the specimen. This reflects that the antibacterial activity of the corresponding organoclays strongly depends on the CA loading.

The antibacterial activity of organic antibacterial materials strongly depends on their sorption ability to bacteria. An increase of CA content results in two significant effects on the property of the resultant organoclays. One is that the increase of CA loading will lead to an increase of hydrophobicity of the resultant organoclays. The increase of hydrophobicity improves the affinity between the organoclays and *E. coli* [44]. On the other hand, the cell walls of the viable bacteria are usually negatively charged due to functional groups such as carboxylates present in lipoproteins at the surface [45]. The increase of the intercalated CA cations increases the electrostatic force between the organoclays and bacteria, and immobilizes the bacteria on the surface of the organoclays. Accordingly, the antibacterial activity of the resultant organoclays increases with an increase of the CA loading. Fig. 9(7) is the halo test result of CaMt-2.0CEC one year later. The clearly recorded halo circle demonstrates that the antibacterial activity of the organoclays can last for a long period. It is of high importance for the application of organoclays with antibacterial activity.

4. Conclusions

In this study, a novel organoclay with antibacterial activity was synthesized using Ca-montmorillonite and Chlorhexidini Acetas. Since Chlorhexidini Acetas has dual characteristics of cationic surfactant and antibacterial activity, the resultant organoclays will be of potential use in the synthesis of organoclay-based materials with antibacterial activity.

XRD patterns in combination with TG results demonstrate that CA ions have been intercalated into clay interlayer. The arrangement of CA ions within the interlayer of the organoclay prepared at 0.2 CEC belongs to a lateral monolayer. On the other hand, CA ions are supposed to be in "kink" state or a special state with partial overlapping in those organoclays prepared at 1.0–4.0 CEC. The intercalation of CA into the clay interlayer, indicated by the basal spacing, is also supported by the fact of a prominent shift of Si–O and Si–O–Si vibrations and the unchange of the wavenumber of Al–OH and Mg–O bending vibrations. HRTG analysis demonstrates that the CA locating outside clay interlayer exists in all resultant organoclays, resulted from the complex molecular configuration of CA. The dramatic decrease of the surface sorbed water and interlayer hydrated water is caused by the surface property transformation and the replacement of hydrated cations by cationic surfactant, respectively. Antibacterial activity test against *E. coli* demonstrates that the raw montmorillonite and the organoclay complex prepared at a low CA concentration (0.2 CEC) do not show antibacterial activity. The antibacterial activity of the resultant organoclays strongly depends on the CA loading, i.e., the antibacterial activity of the resultant organoclays increases with the increase of CA loading. After one year, the halo test demonstrates that the resultant organoclays still show excellent antibacterial activity, indicating that the antibacterial activity of the organoclays can last for a long period. It is of high importance for the application of synthesized antibacterial materials.

Acknowledgments

This work was funded by Natural Science Foundation of Guangdong Province (Grant No. 023203) and Scientific and Technological Project of Guangdong Province China (Grant No. 013109). The Inorganic Materials Research Program, Queensland University of Technology, is gratefully acknowledged for infra-structural support.

References

[1] F. Bergaya, G. Lagaly, Appl. Clay Sci. 19 (2001) 1.
[2] S.S. Ray, M. Okamoto, Prog. Polym. Sci. 28 (2003) 1539.
[3] L.Z. Zhu, B.L. Chen, X.Y. Shen, Environ. Sci. Technol. 34 (2000) 468.
[4] M.O. Adebajo, R.L. Frost, J.T. Kloprogge, O. Carmody, J. Porous Mater. 10 (2003) 159.
[5] G. Lagaly, Clay Miner. 16 (1981) 1.
[6] J.X. Zhu, H.P. He, J.G. Guo, D. Yang, X.D. Xie, Chin. Sci. Bull. 48 (2003) 368.
[7] R.A. Vaia, R.K. Teukolsky, E.P. Giannelis, Chem. Mater. 6 (1994) 1017.
[8] Y.Q. Li, H. Ishida, Langmuir 19 (2003) 2479.
[9] H.P. He, R.L. Frost, J.X. Zhu, Spectrochim. Acta A 60 (2004) 2853.
[10] H.P. He, R.L. Frost, Y.F. Xi, J.X. Zhu, J. Raman Spectrosc. 35 (2004) 316.
[11] Y.Q. Li, H. Ishida, Chem. Mater. 14 (2002) 1398.
[12] W. Xie, Z.M. Gao, K.L. Liu, W.P. Pan, R. Vaia, D. Hunter, A. Singh, Thermochem. Acta 339 (2001) 367.
[13] W. Xie, Z.M. Gao, W.P. Pan, D. Hunter, A. Singh, R. Vaia, Chem. Mater. 13 (2001) 2979.
[14] W. Xie, R.C. Xie, W.P. Pan, D. Hunter, B. Koene, L.S. Tan, R. Vaia, Chem. Mater. 14 (2002) 4837.
[15] S. Yariv, Appl. Clay Sci. 24 (2004) 225.
[16] H.P. He, Z. Ding, J.X. Zhu, P. Yuan, Y.F. Xi, D. Yang, R.L. Frost, Clays Clay Miner. 53 (2005) 287.
[17] H.P. He, R.L. Frost, F. Deng, J.X. Zhu, X.Y. Weng, P. Yuan, Clays Clay Miner. 52 (2004) 350.
[18] J.X. Zhu, H.P. He, L.Z. Zhu, X.Y. Weng, F. Deng, J. Colloid Interface Sci. 286 (2005) 239.
[19] S.Y. Lee, S.J. Kim, Colloids Surf. A 211 (2002) 19.
[20] S.Y. Lee, S.J. Kim, Clays Clay Miner. 50 (2002) 435.
[21] H.P. He, R.L. Frost, T. Bostrom, P. Yuan, L. Duong, D. Yang, Y.F. Xi, T.J. Kloprogge, J. Colloid Interface Sci. (2005), in press.
[22] Y.L. Ma, Z.R. Xu, T. Guo, P. You, J. Colloid Interface Sci. 280 (2004) 283.
[23] F. Ohashi, A. Oya, Appl. Clay Sci. 6 (1992) 301.
[24] F. Ohashi, A. Oya, L. Duclaux, F. Beguin, Appl. Clay Sci. 12 (1998) 435.
[25] B.W. Li, S.H. Yu, J.Y. Hwang, S.Z. Shi, J. Miner. Mater. Character. Eng. 1 (2002) 61.
[26] Y.H. Zhou, M.S. Xia, Y. Ye, C.H. Hu, Appl. Clay Sci. 27 (2004) 215.
[27] P.W.R. Osinaga, R.H.M. Grande, R.Y. Ballester, M.R.L. Simionato, C.R.M. Rodrigues, A. Muench, Dental Mater. 19 (2003) 212.
[28] H.P. He, J.G. Guo, X.D. Xie, J.L. Pen, Environ. Int. 26 (2001) 347.
[29] S. Shani, M. Friedman, D. Steinberg, Caries Res. 34 (2000) 260.
[30] A. Oya, T. Banse, F. Ohashi, S. Otani, Appl. Clay Sci. 6 (1991) 135.
[31] H. Favre, G. Lagaly, Clay Miner. 26 (1991) 19.
[32] H.P. He, J. Galy, J.F. Gerard, J. Phys. Chem. B 109 (2005) 13301.
[33] R.E. Grim, Clay Mineralogy, McGraw–Hill, New York, 1968.
[34] W.Z. Xu, C.T. Johnston, P. Parker, S.F. Agnew, Clays Clay Miner. 48 (2000) 120.
[35] J. Madejova, M. Janek, P. Komadel, H.J. Herbert, H.C. Moog, Appl. Clay Sci. 20 (2002) 255.
[36] V.C. Farmer, The Infrared Spectra of Minerals, The Mineralogical Society, London, 1974.

[37] L. Yan, C.B. Roth, P.F. Low, Langmuir 12 (1996) 4421.
[38] L. Yan, P.F. Low, C.B. Roth, Clays Clay Miner. 44 (1996) 749.
[39] C.T. Johnston, G. Sposito, C. Erickson, Clays Clay Miner. 40 (1992) 722.
[40] Q.H. Zeng, A.B. Yu, G.Q. Lu, R.K. Standish, Chem. Mater. 15 (2003) 4732.
[41] Q.H. Zeng, A.B. Yu, G.Q. Lu, R.K. Standish, J. Phys. Chem. B 108 (2004) 10025.
[42] N.V. Venkataraman, S. Vasudevan, J. Phys. Chem. B 105 (2001) 1805.
[43] S. Barman, N.V. Venkataraman, S. Vasudevan, R. Seshadri, J. Phys. Chem. B 107 (2003) 1875.
[44] P. Herrera, R.C. Burghardt, T.D. Phillips, Vet. Microbiol. 74 (2000) 259.
[45] P.J. Breen, C.M. Compadre, E.K. Fifer, H. Salari, D.D. Serbus, D.L. Lattin, J. Food Sci. 60 (1995) 1191.